PCCP

Shear adhesive strength between epoxy resin and copper surfaces: a density functional theory study

Journal:	*Physical Chemistry Chemical Physics*
Manuscript ID	CP-ART-07-2022-003354.R1
Article Type:	Paper
Date Submitted by the Author:	11-Oct-2022

Complete List of Authors:	Sumiya, Yosuke; Kyushu University, Institute for Materials Chemistry and Engineering Tsuji, Yuta; Kyushu University, Faculty of Engineering Sciences Yoshizawa, Kazunari; Kyushu University, Institute for Materials Chemistry and Engineering

ARTICLE

Shear adhesive strength between epoxy resin and copper surfaces: a density functional theory study†

Received 00th January 20xx,
Accepted 00th January 20xx

DOI: 10.1039/x0xx00000x

Yosuke Sumiya,[a] Yuta Tsuji [b] and Kazunari Yoshizawa*[a]

Adhesive strength varies greatly with direction; various adhesion tests have been conducted. In this study, the shear and tensile adhesive strength of epoxy resin for copper (Cu) and copper oxide (Cu_2O) surfaces were estimated based on quantum chemical calculations. Here, density functional theory (DFT) calculations with dispersion correction were used. In the tensile process, the entire epoxy resin is peeled off vertically, whereas in the shear process, a force parallel to the adhesive surface is applied. Then, a bending moment acts on the adhesive layer, and a total force (stress) inclined at an angle θ with respect to the adherend surface is applied to the adhesive interface. We computed adhesive stress-displacement curves for each θ exhaustively and discussed the changes. When θ equals 90°, it corresponds to a tensile process. As θ decreases from 90°, the shear adhesive stress on both surfaces decreases slowly. When θ is less than 30°, the constraint to the surface causes periodic changes in the adhesive stress curves. The constraint to the Cu_2O surface is especially strong, and this change is large. This periodicity is similar to the stick-slip phenomenon in tribology. To further understand the shear adhesive forces, force decomposition analysis was performed, revealing that the periodicity of the adhesive stress originates from the DFT contribution rather than dispersion one. The procedure proposed in this study for estimating shear adhesive strength is expected to be useful in the evaluation and prediction of adhesive and adherend properties.

1. Introduction

In recent years, demands for light weight and cost reduction of products and devices such as airplanes, automobiles and precision machinery have been increasing from the viewpoint of energy saving and global environmental protection.[1-4] To meet these demands, adhesive technology using adhesives has been attracting attention. Adhesives are inexpensive, lightweight, and used in a wide range of industries. Adhesives are classified based on their main components and curing methods, and are selected according to the properties of the adherend and the application. One of the most typical adhesives is epoxy resin. Epoxy resins are used in many manufacturing processes such as pultrusion, moulding, and coating.[5]

Epoxy resins are synthesized through the polymerization reaction of diglycidyl ether of bisphenol A (DGEBA) shown in Fig. 1a.[6] The adhesion mechanism of epoxy resins has been extensively studied both theoretically and experimentally.[7-33] At the adhesive interface, the ether group, hydroxy group, and benzene ring of DGEBA play important roles, and their interaction with the adherend surface generates adhesive strength. The structure of the adherend surface also has a significant influence on the interaction.

The strength of the interaction at the interface is evaluated based on the adhesive strength, which is the criterion for selecting an adhesive. Adhesive strength is generally measured by adhesion tests defined by the American Society for Testing and Materials (ASTM). Since it is known that adhesive strength varies greatly depending on the direction of external forces applied to the adhesive interface, various tests have been proposed to evaluate adhesive strength in different directions. Fig. 2a and 2b show examples of test to measure tensile and shear adhesion forces, respectively. Although theoretical studies on adhesive strength have also been conducted, most of them are related to tensile adhesive strength.[7-15,19,21,23,24,27,28] Theoretical studies on adhesion forces for different directions have recently been conducted,[18,20,30] but further theoretical analysis of adhesion forces in various directions and its molecular understanding are required.

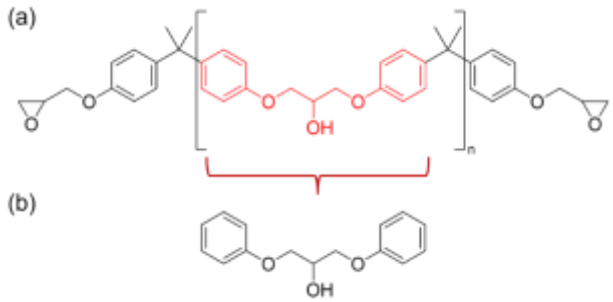

Fig. 1 (a) Chemical structure of bisphenol A epoxy resin. (b) Fragmented model of epoxy resin, which corresponds to the red part in (a).

[a] *Institute for Materials Chemistry and Engineering and IRCCS, Kyushu University, Nishi-ku, Fukuoka 819-0395, Japan. E-mail: kazunari@ms.ifoc.kyushu-u.ac.jp*
[b] *Faculty of Engineering Sciences, Kyushu University, 6-1, Kasuga-koen, Kasuga, Fukuoka, 816-8580, Japan.*
† Electronic Supplementary Information (ESI) available: See DOI: 10.1039/x0xx00000x

In this study, we focused on the shear process and calculated its adhesion force based on first-principles density functional theory (DFT) and compared its results with the tensile adhesion force. The adhesive strength was calculated for epoxy resin/Cu(111) and epoxy resin/Cu_2O(111) interfaces. Note that metallic copper materials have a wide range of industrial applications. An example is a lead frame material in the assembly of semiconductor packages.[34] Since epoxy resin is used to bond semiconductor chips to lead frames, the adhesive interface between the copper surface and epoxy resin has attracted attention. This adhesive strength is reported to be stronger when the copper lead frame surface is oxidized,[35] and the strength of the interaction is evaluated based on shear adhesion strength. Therefore, in this study, we analysed these adhesion processes.

2. Computational method

2.1 Modelling of the epoxy resin adsorbed on Cu(111) surface

In this study, all the DFT calculations were performed using the Vienna Ab initio Simulation Package (VASP) 5.4.4.[36-38] The Perdew-Burke-Ernzerhof form of the generalized gradient approximation (GGA-PBE)[39] was adopted as the exchange correlation functional. The D3 method by Grimme was used for dispersion correction.[40,41] The electron-ion interaction was treated with the Projector Augmented Wave scheme.[42,43] The cut-off energy of the plane wave basis set and the convergence threshold of the self-consistent field calculation were set to 500 eV and 1.0×10^{-5} eV, respectively. The Brillouin zone was sampled with a spacing between k points of $2\pi \times 0.05$ A^{-1}, and the threshold for the atomic force was set to 0.05 eV A^{-1}.

A surface slab model of copper was created according to the following procedure. First, we optimized the unit cell of the bulk copper structure using DFT calculations. The optimized face-centred cubic structure of copper is shown in Fig. S1a. We cut the (111) plane out of the optimized copper structure and constructed a surface slab model of copper. The (111) plane of the face-centred cubic lattice has the highest density and the lowest energy. A rectangular supercell consisting of three atomic layers was then created under periodic boundary condition, and a vacuum layer of about 30 Å thickness was inserted on the surface, resulting in a $15.1 \times 8.7 \times 35.0$ $Å^3$ cell. This slab model contains a total of 72 atoms. The slab model structure was optimized by fixing the Cu atoms in the bottom two layers (Fig. 3a). Structures were visualized using the VESTA software package.[44]

The epoxy resin was modelled by fragmenting the DGEBA structure as shown in Fig. 1b. In this study, this fragment model is referred to as the epoxy molecule. The adsorption structure of the epoxy molecule on the Cu(111) surface was explored by the following procedure. First, the epoxy molecule was randomly

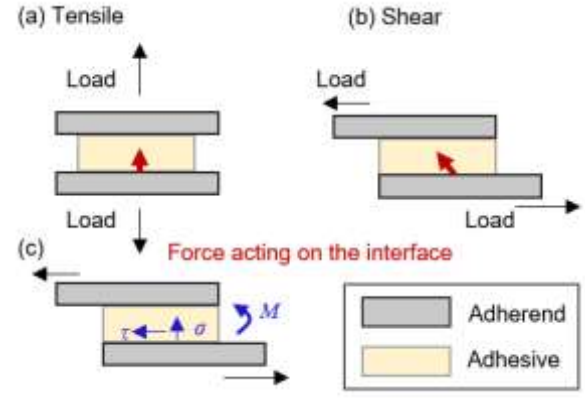

Fig. 2 Typical examples of adhesion tests defined by the American Society for Testing and Materials (ASTM). (a) and (b) are tests to measure tensile and shear adhesive forces, respectively. The net forces acting on the adhesive interfaces under external forces in the tensile and shear directions are indicated by the red arrows. (c) shows the shear stress τ, normal (peel) stress σ, and bending moment M applied to the adhesive layer during the shear process.

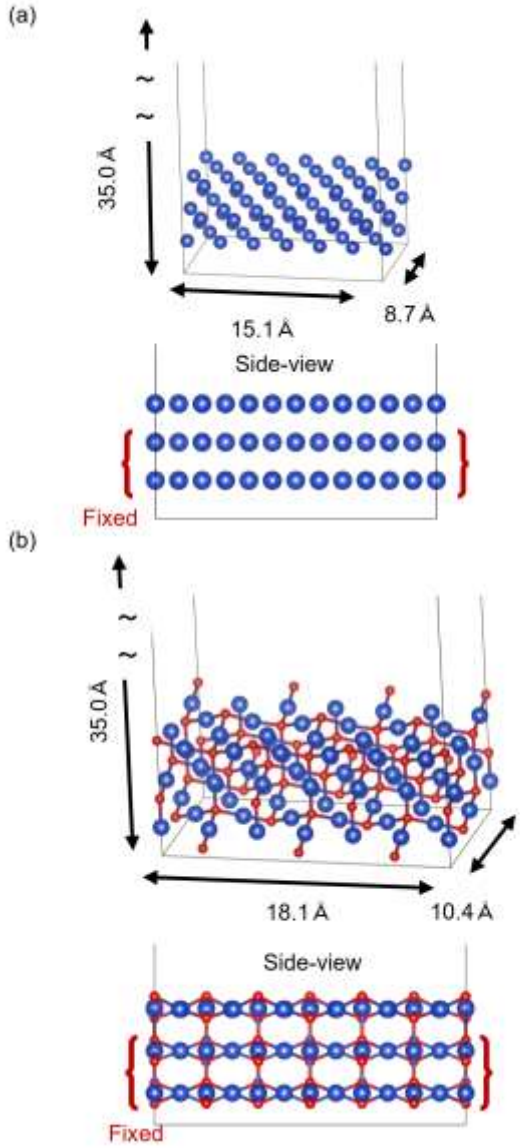

Fig. 3 (a) Cu(111)-surface slab model (b) Cu_2O(111)-surface slab model. Blue represents copper atoms and red represents oxygen atoms.

placed on the Cu(111) surface and optimized with molecular mechanics calculations using the Forcite module of Materials Studio software,[45] where the COMPASS force field[46] was used. Next, quench dynamics simulation was performed to obtain as stable an adsorption structure as possible for the epoxy molecule. The structure obtained was then used as the initial structure for the DFT-level optimization.

In the quench dynamics, low energy structures are explored by sequentially repeating molecular dynamics (MD) simulation and geometry optimization. After the optimization, the resulting stable structure is saved, and a subsequent MD simulation is performed from the structure. The calculations were performed on an NVT ensemble with a Nose-Hoover thermostat[47] at 1000 K, and a time step of 1.0 fs, with time evolution up to 5.0 ns considered. During the quench dynamics, all copper atoms were fixed. Optimization was performed every 50.0 ps, and a total of 100 structures were output. Among the obtained structures, 20 stable structures were reoptimized with DFT, and the most stable structure was used as a model for analysing the adhesion (Fig. 4a). In the optimization by DFT, the Cu atoms in the bottom two layers were fixed as in Fig. 3. The sensitivity of the energy to the number of layers to be fixed is shown in Table S7. The total DFT energy for the obtained structure of the epoxy/Cu(111) surface is shown in Fig. S8. The models made by the above procedure most simply describe the interaction between the epoxy resin and the surface. Here, since only single epoxy molecule is considered, the effects of epoxy resin entanglement and thickness of epoxy resin are neglected. Modelling to incorporate these effects is a future work.

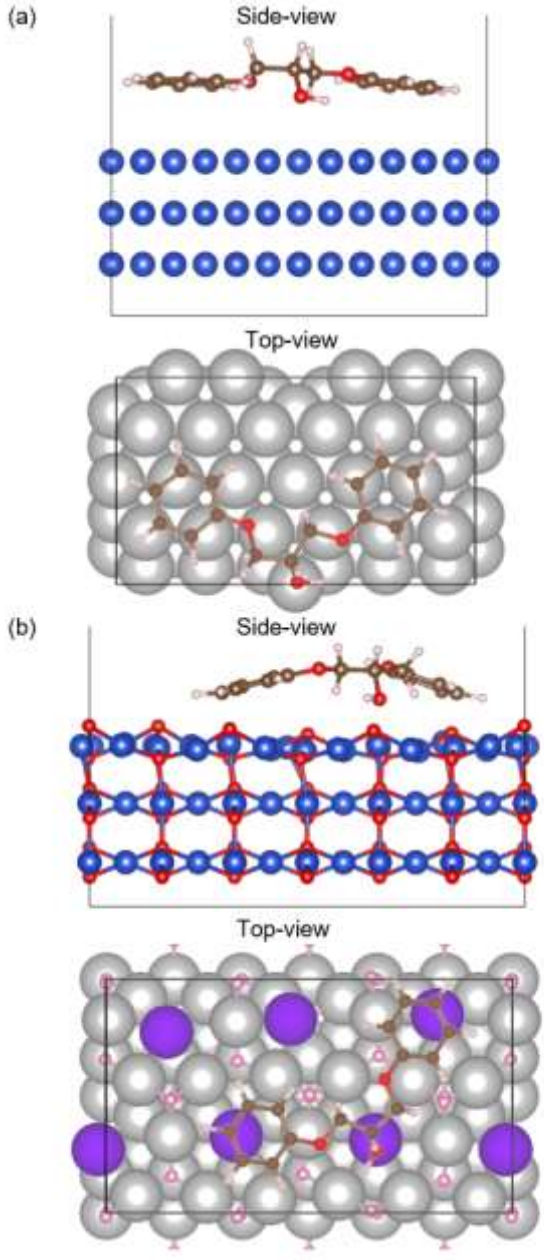

Fig. 4 Adsorption structures of epoxy molecules on (a) Cu(111) and (b) Cu_2O(111) surfaces. The gray and pink atoms in the top-view correspond to copper and oxygen atoms, respectively; the purple atoms correspond to coordinatively unsaturated copper atoms.

2.2 Modelling of the epoxy resin adsorbed on Cu_2O(111) surface

Metallic copper is easily oxidized in air, forming a dense oxide film of Cu_2O on its surface. Cu_2O films form below 150°C and are used as lead frame materials.[48] It is known that above 300°C, a sparse oxide film of CuO forms,[49] resulting in poor adhesion. Therefore, we chose to treat Cu_2O surface, which is often used as a copper material.

In modelling of the copper oxide (Cu_2O) (111) surface, the procedure used to make the copper surface slab model was followed. Here, the cutoff energy was set to 520 eV as previously

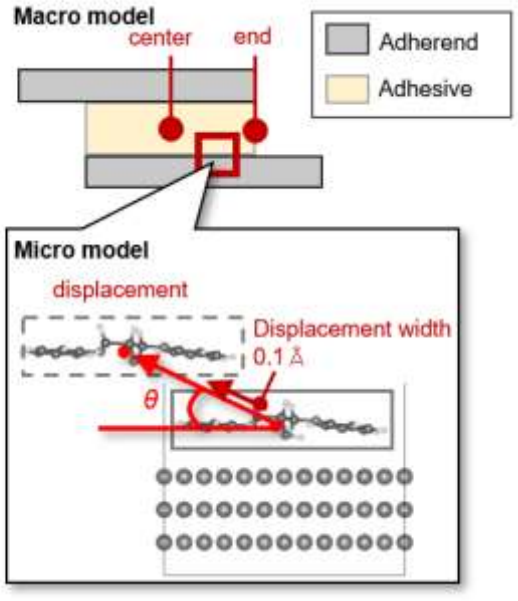

Fig. 5 Relationship between the macro and micro models. In the micro model, the epoxy molecule is displaced by 0.1 Å along the direction of stress represented by the red arrow. The red circle represents the centre of gravity of the epoxy molecule, and θ is the angle of displacement of the epoxy molecule with respect to the surface.

reported.[50] The optimized face-centred cubic structure of Cu_2O is shown in Fig. S1b, where the $Cu_2O(111)$ has two types: an oxygen (O)-terminated nonpolar surface and a copper (Cu)-terminated polar surface. The O-terminated surface is reported to have a lower energy than the Cu-terminated.[51] The O-terminated was selected for this study. A vacuum layer of about 30 Å thickness was inserted on the surface, resulting in a cell size of $18.1 \times 10.4 \times 35.0$ Å^3. The bottom two layers of the Cu_2O slab model were fixed, and the structure of the $Cu_2O(111)$ surface slab model was optimized (Fig. 3b). This slab model contains a total of 108 atoms. The adsorption structure of the epoxy molecule on the surface is shown in Fig. 4b, which was obtained by the same procedure used to create the adsorption structure on the Cu(111) surface. The total DFT energy for the obtained structure of the epoxy/$Cu_2O(111)$ surface is shown in Fig. S8.

Here, the $Cu_2O(111)$ surface is under ideal conditions and the adsorption of impurity molecules is not taken into account. Coordinatively unsaturated copper atoms on the surface are highly active, and water molecules[52,53] and carbon dioxide molecules[54,55] in the air can be adsorbed. Furthermore, in factories that handle adhesives, the surface of adherends is often contaminated with oil. In practical application, the effects of oil stains cannot be ignored. Investigation of these effects is a future work.

2.3 Computational methods for the calculation of shear and tensile adhesion strength

During the shear process, the adhesive is pulled in a direction parallel to the adherend surface, as shown in Fig. 2b. Here, it is assumed that interface fracture occurs between the adhesive and the bottom adherend surface. It is known that adhesives are subjected to a bending moment M.[56,57] This induces a vertical normal (peel) stress σ at the adhesive interface during a shear process. The total stress of σ and shear stress τ acts on the interface, and its direction is inclined toward the adhesive surface (Fig. 2b).

To estimate the shear adhesion force along this direction, a micro-model that explicitly considers molecular interactions was cut out of the macroscopic adhesion model shown in Fig. 5. Here, the gray rectangles in Fig. 5 represent the adherends and the yellow rectangle represents the adhesive. The micro-model corresponds to the complex of the epoxy resin fragment model/surface model created in sections 2.1 and 2.2 (Fig. 4), with one fragment model cut out of the adhesive molecules and three layers from the adherend surface in the area containing the entire fragment model. The shear and tensile adhesion forces were estimated by applying DFT calculations to this micro-model according to the following procedure.

The shear adhesion force in the direction of the red arrow is obtained by differentiating the potential energy curve for the dissociation process of the entire epoxy molecule from the surface along that direction. The angle θ at which the epoxy molecule is displaced from the surface is defined as the shear angle. θ varies with the position from which the micro-model is cut out. At the endpoint of the adhesive layer shown in Fig. 5, M acts strongly on the interface[57-59] and σ becomes large. Thus, θ approaches 90°. In contrast, at the centre, σ becomes weak and θ approaches 0°. In this study, shear adhesion forces for $0° \leq \theta \leq 90°$ were calculated.

At $\theta = 90°$, the dissociation process of the epoxy molecule corresponds to the tensile process in Fig. 2a. The case for $\theta = 0°$ represents the migration process of the epoxy molecule on the surface, and its displacement direction is to the left in the top-view of Fig. 4. We obtained the energy-displacement (ΔE - Δr) plot by performing single point calculations at each point with a displacement width of 0.1 Å.

For large θ, this potential energy curve can be fitted with a Morse potential as follows:

$$E = D(1 - \exp(-a\Delta r))^2 \quad (1)$$

where D is the adhesion energy and a is a constant inherent to the system and related to the width of the potential well. The range of θ that can be fitted by the Morse potential is discussed later. To obtain the adhesion force-displacement (F - Δr) curve, the fitted potential energy curve was differentiated with respect to Δr.

$$F = -\frac{\partial E}{\partial \Delta r} \quad (2)$$

The adhesive force is estimated from the maximum value of F, F_{max}. The maximum value of adhesive stress S, S_{max}, is obtained by dividing F_{max} by the area of the cell, A_{cell}.

$$S_{max} = \frac{F_{max}}{A_{cell}} \quad (3)$$

On the other hand, when θ is a small value, the epoxy molecule is strongly bounded to the surface. In particular, the case of $\theta = 0$ corresponds to the process of migration of the epoxy molecule on the surface, and multiple energy barriers and metastable adsorption structures appear during the displacement. For such a process, the potential energy curve cannot be fitted with eqn (1). Therefore, we fitted the energy curve using the following equation, which is based on the Morse potential with a correction term:

$$E = D(1 - \exp(-a(\Delta r - \alpha)))^2 + \sum_{i=1}^{n} b_i \cos(c_i \Delta r - d_i) + \beta \quad (4)$$

where α, β, b_i, c_i, and d_i are fitting parameters, and n is set to 5 in this study. The second term is the Fourier cosine series, which is used for fitting periodic functions with even function properties. Even using eqn (4), the corresponding adhesive forces can be estimated from eqn (2) and (3). Using the above equations, we calculated ΔE and S for the adsorption structures in Fig. 4a and 4b to make Δr - θ - ΔE and Δr - θ - S surfaces.

3. Results and discussion

3.1 Shear adhesive strength of the epoxy molecule for the Cu(111) and $Cu_2O(111)$ surfaces

The shear angle θ in the micro model in Fig. 5 varies with the cut-out position from the macro model. In the shear process, it is

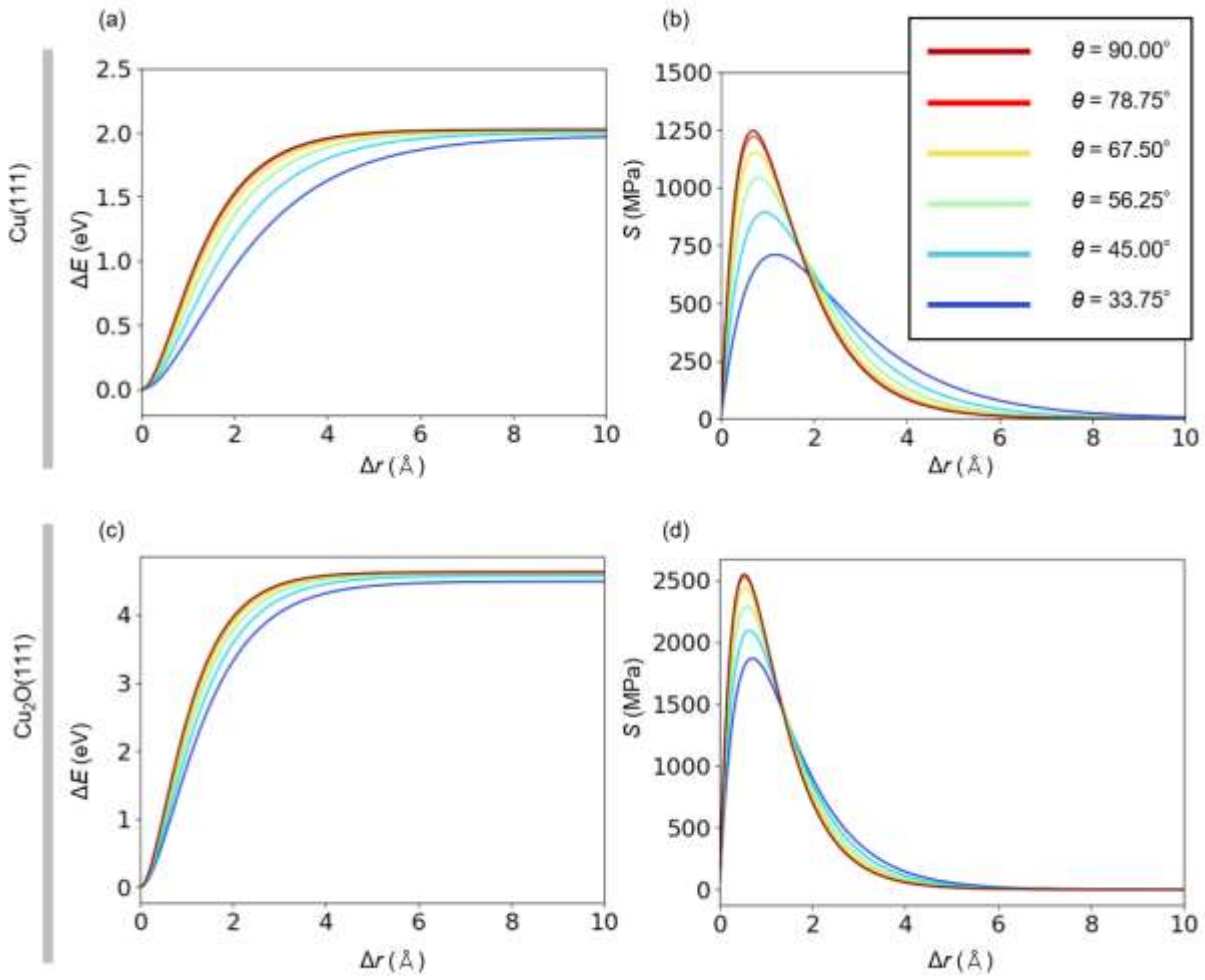

Fig. 6 (a) and (b) show the energy and adhesive stress curves of the epoxy molecule on the Cu(111) surface. (c) and (d) show the energy and adhesive stress curves of the epoxy molecule on the Cu_2O(111) surface.

known that stronger bending moments M act on the endpoint of the adhesive.[57-59] It is therefore suggested that θ increases with a larger σ in the micro-model cut out from the region close to the endpoint shown in Fig. 5. Based on this discussion, adhesive stress curves were calculated for different θ, from which adhesive stress surfaces for Δr, θ, and S were made.

Fig. 6 shows the energy and adhesive stress curves of the epoxy molecule on the Cu(111) and Cu_2O(111) surfaces at large shear angles ($33.75° \leq \theta \leq 90.00°$). Fig. 6a and 6b show the energy and adhesive stress curves of the epoxy molecule on the Cu(111) surface. Fig. 6c and 6d show the energy and adhesive stress curves of the epoxy molecule for the Cu_2O(111) surface. Here, θ was set in 11.25° increments. The energy changes for displacements up to 10 Å for both surfaces were computed by single point calculations. Each energy curve in the figures was obtained by fitting to eqn (1), and adhesion stress curves were obtained by applying eqn (2) and (3) to the fitting functions. Three-dimensional versions of Fig. 6 are shown in Fig. S2 and S3. The coefficients of determination R^2 for all fittings are greater than 0.99. Plots of the computed values for each θ are also shown in Fig. S4 and S6.

As shown in Fig. 6, S increases with increasing θ on both surfaces. There is one maximum in all adhesion curves. S_{max} at each θ, the displacement Δr_{max} giving S_{max}, and the fitting parameters (D and a) are listed in Table 1. S_{max} is maximum in the tensile process, i.e., when θ = 90°. This suggests that the upper limit of shear adhesive strength can be estimated from the tensile adhesive strength. It is suggested that the shear adhesive stress in the region near the endpoints also increases just as the greater stress acts at the endpoints of the adhesive layer where θ increases.[48,49] In contrast, D does not change with increasing θ, suggesting that adhesive energy is conserved even when the shear angle changes, since D means adhesive energy. Moreover, a increases with increasing θ. The width of the potential well narrows as a increases. This effect results in a smaller value of Δr_{max} with respect to an increase in θ.

Comparing the Cu(111) and Cu_2O(111) surfaces, the adhesive strength on the Cu_2O(111) surface is greater for all θ. This trend is consistent with a previous study that examined the case for θ = 90°.[27] The high adhesive strength on the Cu_2O(111) surface is due to the strong interaction of the OH and Ph groups of the epoxy molecule with the coordinatively unsaturated copper atoms on the surface.[27]

As shown in Table 1, our calculated tensile adhesive stresses were estimated to be 1246 MPa for the Cu(111) surface and 2548 MPa for the Cu_2O(111) surface. These were very large values compared to the adhesive strength of 50 MPa for epoxy/steel[60] and 120 MPa for epoxy/bare-sapphire.[61] Local adhesion stresses estimated by quantum

chemical and molecular dynamics calculations are known to be much larger than those measured macroscopically in laboratory test samples.[62,63] This is due to the assumption that the fragment model of the epoxy resin is adsorbed in the most stable conformation to the surface. If the size of the fragment model for the epoxy resin were larger and the area to be explicitly calculated were larger, the adhesion stresses would be smaller due to conformational constraints. The assumption of an ideal surface also contributes. Further research is needed to improve the quantification for adhesive stress. On the other hand, the framework provided by this study is also useful in the qualitative comparison of adhesive stress between copper and copper oxide, and the affinity between the adhesive and the adherend can be discussed based on first principles.

The essence of first-principles calculations is to discuss the mechanism of interaction from the electron level. The analysis of the Hamilton population of crystal orbitals (COHP)[64] would also be helpful, since it reflects well the changes in the crystal orbitals.[65] The results of COHP calculations for stable adhesion structures are shown in Fig. S9.

3.2 Shear adhesive strength and tribological behaviour of the adhesive molecule on the Cu(111) surface at small shear angles

When the cut-out position for the micro-model is relatively far from the endpoint of the adhesive, the shear angle θ is assumed to be small due to shear stress τ being dominant. When θ is small, the potential energy curve is distorted from the Morse potential type due to binding from the surface. To investigate this change in detail, the analysis was made four times finer by reducing the θ incremental width from 11.2500° to 2.8125°. Fig. 7a and 7b show the energy surface (Δr - θ - ΔE) and energy curves (Δr - ΔE) for the Cu(111) surface in the range of 0.0000° ≤ θ ≤ 33.7500°. Here, the energy change for displacements up to 10 Å was obtained by single point calculations. Each energy curve was obtained by fitting to eqn (4) to account for periodic distortions. The adhesion stress surface (Δr - θ - S) was made by applying eqn (2) and (3) to those fitting functions. The obtained 3 and 2 dimensional plots of the adhesive stress surfaces are shown in Fig. 7c and 7d. The coefficients of determination R^2 for all fittings are greater than 0.99. Each fitting parameter is shown in Table S1. Plots of the computed values for each θ are shown in Fig. S5.

The energy curve at θ = 0.0° represents the migration process of the epoxy molecule on the surface. As seen in Fig. 7a and 7b, the process involves a metastable minimum point next to the initial position, with an activation barrier between them. After surpassing the activation barrier, the sign of the force is negative because it falls to a metastable minimum point. As θ increases, the energy curve gradually approaches the shape of the Morse potential by increasing the energy in the large Δr region. This is due to that the larger θ, the greater the distance between the epoxy molecule and the surface with respect to the increase in Δr, and the weaker the interaction from the surface.

As shown in Fig. 7c and 7d, there are multiple stress maxima in the small θ region. The value of Δr_{max}, which gives the maximum value of adhesive stress, S_{max}, shows different behaviour depending on θ. Table 2 shows S_{max} and Δr_{max}. For θ = 0.0000, 2.8125, and 5.6250°, Δr_{max} corresponds to the first maximum position, and Δr_{max} decreases as θ increases. Then, when θ = 8.4375°, the second maximum point is larger than the first; thus, Δr_{max} corresponds to the position of the second maximum. For θ = 8.4375 to 19.6875°, Δr_{max} becomes smaller for increasing θ. Here, the first and second peaks gradually get mixed. At θ = 22.5000°, the first and second peaks mix to form a single broad peak. For θ = 22.5000 to 33.7500°, Δr_{max} is even smaller.

The adhesive stress curve in the range from θ = 0.0000° to 5.6250° has a periodicity. This feature is common to frictional forces. In tribology, the stick-slip phenomenon, in which a periodic frictional force acts on an object moving on a surface at a constant speed, is known.[66] The behaviour of periodic oscillations of the force of a molecule sliding (θ = 0.0000°) on a surface has been confirmed both experimentally and theoretically.[67-73] To investigate the origin of these forces, the energy and adhesive force at θ = 0.0000° and 2.8125° were decomposed into two terms expressed as follows:

$$E_{\mathrm{DFT+disp}} = E_{\mathrm{DFT}} + E_{\mathrm{disp}} \quad (5)$$

$$F_{\mathrm{DFT+disp}} = F_{\mathrm{DFT}} + F_{\mathrm{disp}} \quad (6)$$

where E_{DFT} and E_{disp} represent the DFT and dispersion energies, respectively, and F_{DFT} and F_{disp} represent the DFT and dispersion forces, respectively.

Fig. 8a and 8b show the energy and adhesive stress curves at θ = 0.0000°, and Fig. 8c and 8d show the energy and adhesive stress curves at θ = 2.8125°. Each point in the dotted line corresponds to the value obtained by the single-point calculation, and the curves obtained by fitting them are shown by the solid black, blue, and red lines, where black corresponds to the total energy, blue to the dispersion energy, and red to the DFT energy. Here, the blue and red lines are fitted to eqn (7) and (8), respectively.

$$E = \sum_{i=0}^{12} e_i (\Delta r)^i \quad (7)$$

Table 1 S_{max}, Δr_{max}, and fitting parameters for each θ at the epoxy molecule/Cu(111) and epoxy molecule/Cu_2O(111) interfaces.

		Cu(111)		
θ (°)	S_{max} (MPa)	Δr_{max} (Å)	D (eV)	a (Å^{-1})
90.00	1246	0.68	2.03	1.02
78.75	1222	0.69	2.02	1.00
67.50	1155	0.73	2.02	0.94
56.25	1044	0.81	2.01	0.86
45.00	893	0.94	2.00	0.74
33.75	710	1.17	1.98	0.59
		Cu_2O(111)		
θ (°)	S_{max} (MPa)	Δr_{max} (Å)	D (eV)	a (Å^{-1})
90.00	2548	0.53	4.63	1.30
78.75	2526	0.54	4.63	1.29
67.50	2439	0.56	4.62	1.24
56.25	2292	0.59	4.61	1.17
45.00	2095	0.64	4.58	1.08
33.75	1869	0.71	4.49	0.98

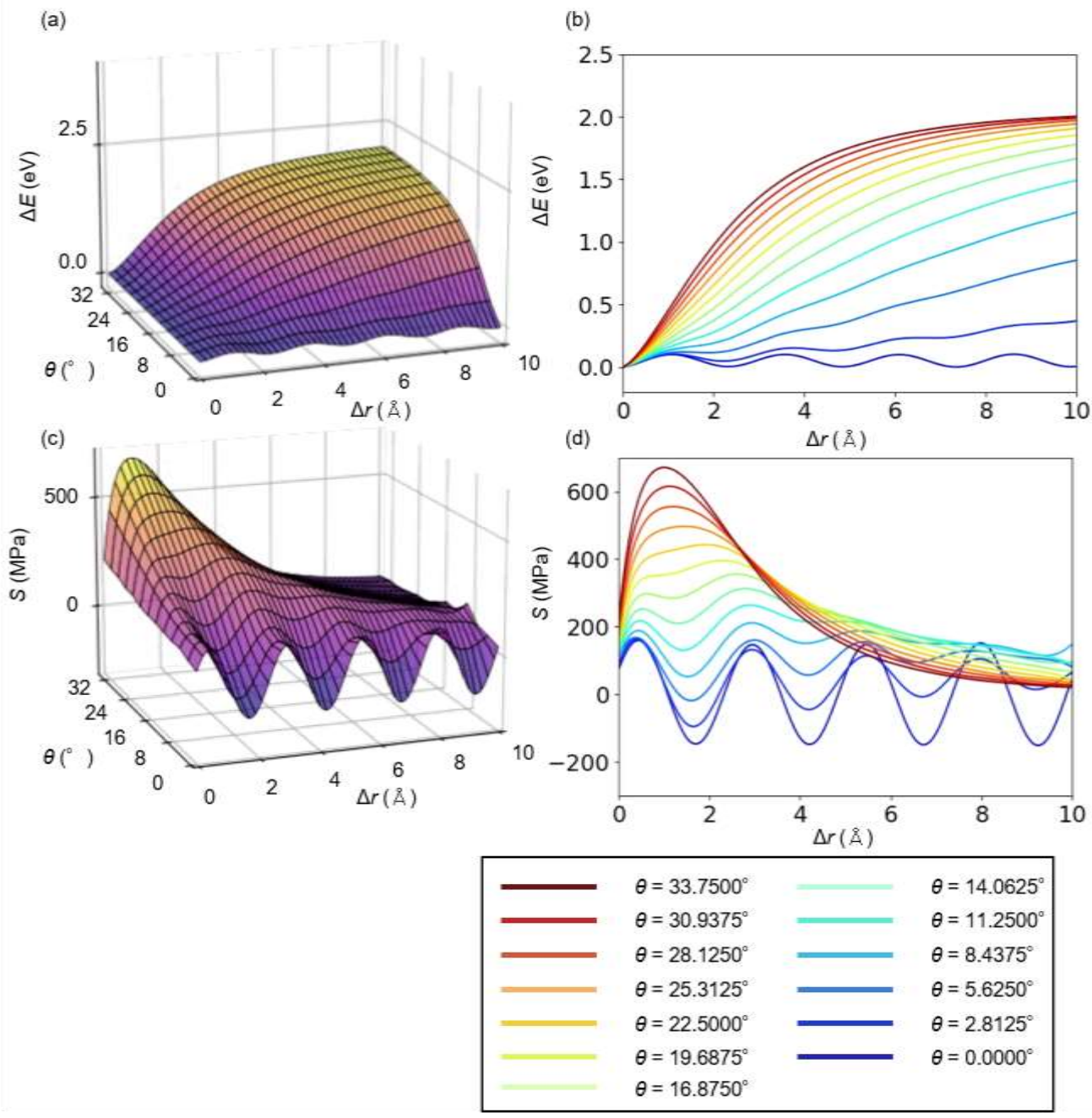

Fig. 7 (a) and (b) show 3D and 2D plots of the energy surface of the epoxy molecule on the Cu(111) surface. (c) and (d) show 3D and 2D plots of shear adhesion stress surface.

$$\boldsymbol{E} = \sum_{i=1}^{5} \boldsymbol{b_i} \cos(\boldsymbol{c_i \Delta r} - \boldsymbol{d_i}) + \boldsymbol{\beta} \qquad (8)$$

Eqn (7) is a polynomial function and e_i is the fitting parameter. Eqn (8) corresponds to the second term in eqn (4), i.e., the correction term for the Morse potential. The coefficients of determination R^2 for these fittings are greater than 0.99. The fitting parameters are shown in Table S1, S3, and S5.

As shown in Fig. 8a, the dispersion energy at θ = 0.0000° is almost zero, and the total and DFT energies are almost the same. The total stress curve also overlaps almost perfectly with the DFT force (Fig. 8b). Therefore, the adhesive strength at θ = 0.0000° was found to originate from the DFT part. At θ = 2.8125°, the dispersion energy increases linearly (Fig. 8c). On the other hand, the DFT energy decreases in an oscillating manner. The sum of the two results in an oscillating increase in the total energy. In the stress curve in Fig. 8d, the dispersion force decreases slowly and the DFT force oscillates in a damped manner. The sum of them results in a damped oscillation of the total force with the large first maximum. The results indicate that both dispersion force and DFT components contribute to the magnitude of the first adhesive stress maximum, but that only the DFT component contributes to the periodic behaviour. This suggests that the origin of the feature common to the stick-slip phenomenon is derived from the DFT component.

3.3 Shear adhesive strength and tribological behaviour of the Cu_2O(111) surface at small shear angles

Table 2 Values of S_{max} and Δr_{max} for each θ at the epoxy molecule/Cu(111) interface.

θ (°)	S_{max} (MPa)	Δr_{max} (Å)
33.7500[1]	671[1]	1.00[1]
30.9375	615	1.13
28.1250	556	1.20
25.3125	497	1.45
22.5000	443	1.92
19.6875	396	2.28
16.8750	355	2.61
14.0625	313	2.79
11.2500	264	2.89
8.4375	211	2.94
5.6250	168	0.38
2.8125	164	0.39
0.0000	160	0.44

[1]These values were obtained by fitting to eqn (4) and therefore differ slightly from the ones obtained by fitting to eqn (1), which are shown in Table 1.

Fig. 9a and 9b show the energy surface (Δr - θ - ΔE) and energy curves (Δr - ΔE) for the Cu_2O(111) surface in the range of $0.0000° \leq \theta \leq 33.7500°$. Here, the energy changes for displacements up to 18 Å were computed using single point calculations. Each energy curve in the figures is obtained by fitting to eqn (4) and the adhesive stress surface (Δr - θ - S) by eqn (2) and (3). A three-dimensional plot of the adhesive stress surface is shown in Fig. 7c and a two-dimensional plot in Fig. 7d. The coefficients of determination R^2 for all fittings are greater than 0.99. Each fitting parameter is shown in Table S2. Plots of the computed values for each θ are shown in Fig. S7. The values of S_{max} and Δr_{max} for each θ are shown in Table 3.

For the Cu_2O(111) surface, the energy barriers at $\theta = 0.0000°$ are very large. The structures corresponding to the minima and maxima on the energy curve at $\theta = 0.0000°$ in Fig. 9b are shown at **1**-**7** in Fig. 10. Here, the coordinatively unsaturated copper atoms on the surface close to the epoxy molecule are indicated by yellow crosses. At each of minima **1**, **3**, **5**, and **7**, the

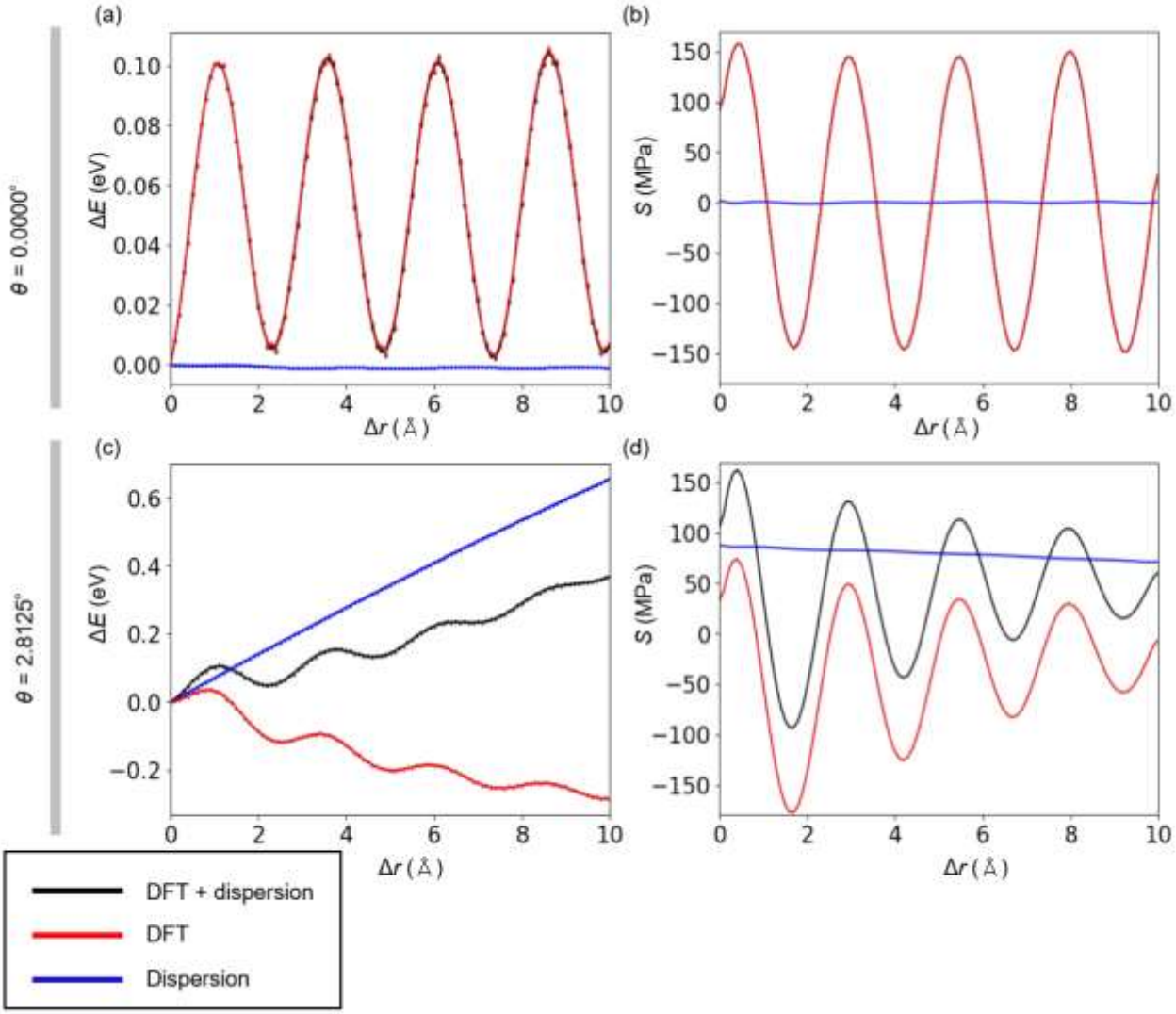

Fig. 8 (a) and (b) show the energy and adhesive stress curves of the epoxy molecule on the Cu(111) surface at $\theta = 0.0000°$. (c) and (d) show the energy and adhesive stress curve at $\theta = 2.8125°$. Each point in the dotted line corresponds to the value obtained by the single-point calculation, and the curves obtained by fitting them are represented as the black, blue, and red solid lines: Black corresponds to total, blue to dispersion, and red to DFT.

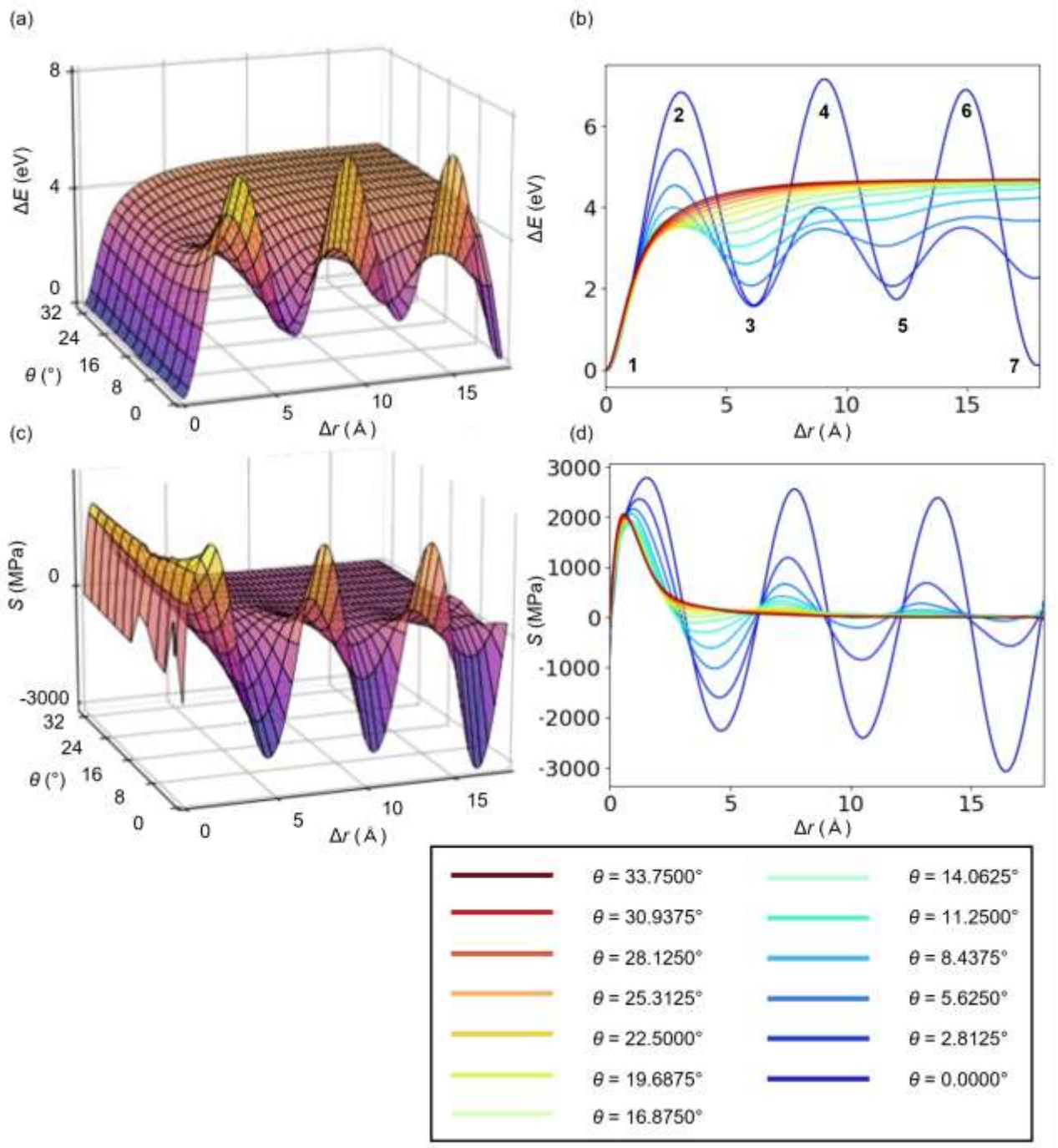

Fig. 9 (a) and (b) show 3D and 2D plots of the energy surface of the epoxy molecule on the $Cu_2O(111)$ surface. (c) and (d) show 3D and 2D plots of shear adhesive stress surface. The structures corresponding to minima **1**, **3**, **5**, and **7** and maxima **2**, **4**, and **6** on the energy curve at $\theta = 0.0000°$ are shown in Fig. 10.

coordinatively unsaturated copper atoms are close to the Ph and OH groups of the epoxy molecule and strongly interact with them. On the other hand, at maxima **2**, **4**, and **6**, the Ph and OH groups of the epoxy molecule are located between the coordinatively unsaturated copper atoms and the interactions are weak. It has been reported that the interaction between a coordinatively unsaturated copper atom and a Ph group is a coordinate bond, and the interaction between a coordinatively unsaturated copper atom and an OH group is a σ bond via a p-d orbital interaction.[27] It was found that these chemical bonds provide a larger contribution to the DFT energy rather than the dispersion energy, and are the origin of the large energy barrier at $\theta = 0.0000°$. This is supported by the fact that the DFT-derived force is almost zero in the case of no chemical bonding at the interface.[24] It is thus suggested that the epoxy molecule is not easily displaced at small shear angles near $\theta = 0.0000°$. The feature that the energy curve gradually approaches the Morse

Table 3 Values of S_{max} and Δr_{max} for each θ at the epoxy molecule/Cu_2O(111) interface.

θ (°)	S_{max} (MPa)	Δr_{max} (Å)
33.7500[1]	2065[1]	0.60[1]
30.9375	2027	0.62
28.1250	1994	0.64
25.3125	1967	0.66
22.5000	1947	0.68
19.6875	1937	0.71
16.8750	1939	0.74
14.0625	1855	0.86
11.2500	1925	0.91
8.4375	2064	0.91
5.6250	2164	1.00
2.8125	2363	1.24
0.0000	2785	1.54

[1]These values were obtained by fitting to eqn (4) and therefore differ slightly from the ones obtained by fitting to eqn (1), which are shown in Table 1.

potential shape as θ increases is similar to that for the Cu(111) surface, while larger θ is required for the Cu_2O(111) surface.

S_{max} corresponded to the value of the first peak top at all θ. S_{max} value decreases as θ increases from θ = 0.0000 to 14.0625°. At θ = 14.0625°, S_{max} reaches a minimum value (1855 MPa), and the S_{max} value increases with further increase in θ. These results suggest that interface failure is more likely to occur when the stress acting on the adhesive is at a shear angle near 14°. It is also suggested that the angle giving S_{max} minimum is affected by the magnitude of the energy barrier in the migration process on the surface.

As in the case of the Cu(111) surface, Fig. 11 was obtained by decomposing the energy and adhesive stress at θ = 0.0000° and 2.8125° into the DFT and dispersion contributions. The coefficient of determination R^2 for each fitting is greater than 0.99. Each fitting parameter is shown in Table S2, S4, and S6. As shown in Fig. 11a and 11b, the dispersion energy at θ = 0.0000° is almost zero, and the DFT contribution accounts for all the total energy and stress. This is in common with the case of the Cu(111) surface. At θ = 2.8125°, the dispersion energy increases slowly (Fig. 11c). As in the case of the Cu(111) surface, the DFT energy oscillates in a damped manner. The DFT force is very large relative to the dispersion force, and the total force curve overlaps well with the DFT force even as θ increases. This feature differs from that of the Cu(111) surface. This difference is due to the larger DFT contribution in the interaction for the Cu_2O(111) surface than for the Cu(111) surface.

These results suggest that in the shear process for both Cu(111) and Cu_2O(111) surfaces, when the shear angle is small, the adhesive molecule is constrained to the surface, and periodic changes in adhesive force similar to frictional force appear. The energy and force decomposition analysis also indicate that the periodic adhesive force originates from the DFT contribution. In the case of the Cu(111) surface, both DFT and dispersion forces contribute to the total stress (force). On the other hand, in the case of the Cu_2O(111) surface, the DFT contribution is much larger than the dispersion contribution, and most of the total stress (force) is due to the DFT one.

4. Conclusions

Shear adhesive stresses in the fragment model of epoxy resin on the Cu(111) and Cu_2O(111) surfaces were estimated by using DFT calculations to investigate theoretically how the adhesive force acting between the adhesive and the adherend varies with direction. In the shear process for both surfaces, the range of shear angles θ from 0.0° to 90.0° was exhaustively analysed.

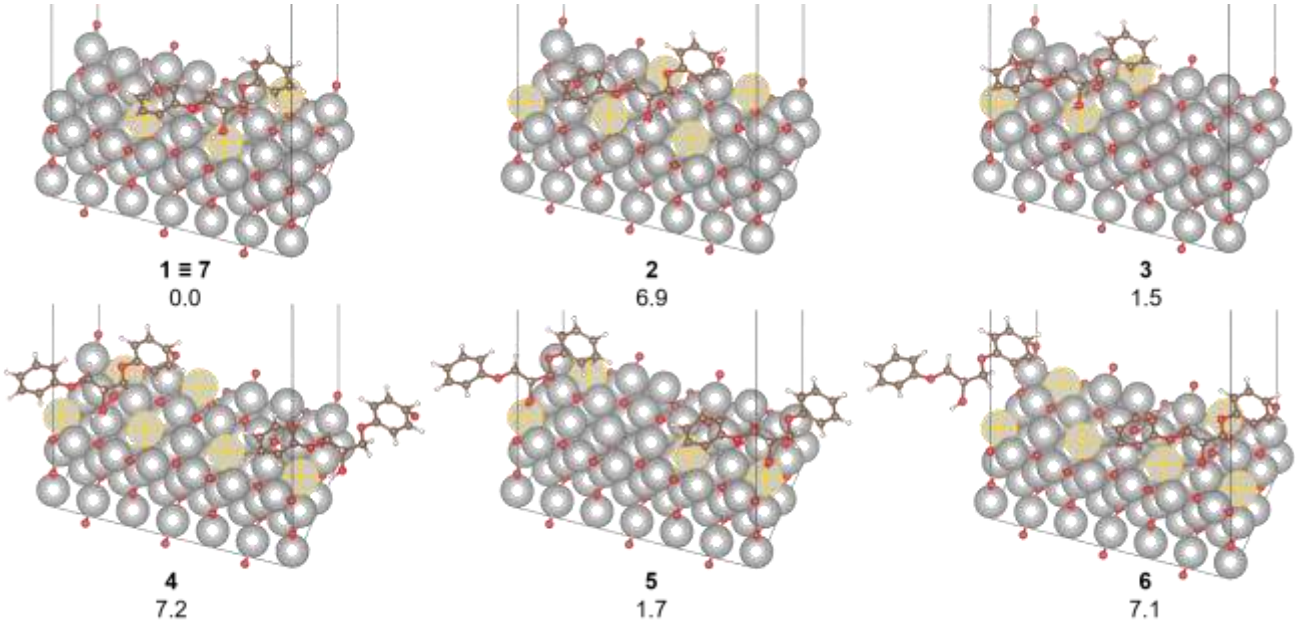

Fig. 10 Stable adsorption structures **1**, **3**, **5**, and **7** at the energy minima and transition structures **2**, **4**, and **6** at the energy maxima obtained by moving the epoxy molecule at θ = 0.0000° on the Cu_2O(111) surface. Coordinatively unsaturated copper atoms close to the epoxy molecule are indicated by yellow crosses. Relative energy values in eV are shown below the structure numbers.

When θ is large ($33.75° \leq \theta \leq 90.00°$), there is one maximum in the adhesive stress curve for each θ. The adhesive strength increases in proportion to θ, and is maximum in the tensile process ($\theta = 90.00°$). It was therefore suggested that the upper limit of shear adhesive strength could be estimated from the tensile adhesive strength. The adhesive stress of the epoxy resin on the $Cu_2O(111)$ surface is greater than that for the Cu(111) surface for all θ values investigated.

When θ is small ($0.00° \leq \theta \leq 33.75°$), the potential energy curve cannot be approximated by a Morse potential due to perturbation to the potential curve caused by strong binding to the surface. The energy curve at $\theta = 0.0°$ corresponds to the process of the epoxy molecule sliding on the surface, with multiple activation barriers and metastable adsorption structures. The shape of the potential energy curve indicates that the adhesive strength varies periodically. This periodicity is common to the stick-slip phenomenon, which is well known in tribology. As θ increases, the energy curve gradually approaches the shape of a Morse potential. The periodicity of the adhesive force gradually disappears; the first maximum remains. One can see the transformation of friction phenomena into adhesion phenomena.

To further understand the features of the shear process when θ is small, a force decomposition analysis was applied to separate the adhesive force into the DFT and the dispersion forces. A common feature for both surfaces is the periodicity of the DFT force curve near $\theta = 0.0°$. The dispersion force is nearly zero at $\theta = 0.0°$. Therefore, it is suggested that the periodicity of the adhesive force is derived from the DFT energy. The magnitude of the DFT force differs significantly between the Cu(111) and $Cu_2O(111)$ surfaces, with the Cu(111) surface resulting in a smaller DFT force. As θ increases, dispersion force is induced, contributing to the magnitude of the total force. On the other hand, the DFT force on the $Cu_2O(111)$ surface is very strong, and most of the total force is due to the DFT contribution. The procedure proposed in this study for estimating shear adhesive strength is expected to be useful in the evaluation and prediction of adhesive and adherend properties.

Conflicts of interest

There are no conflicts to declare.

Acknowledgements

This work was supported by KAKENHI grants (numbers JP21K04996 and JP22H00335) from the Japan Society for the Promotion of Science (JSPS) and the Ministry of Education, Culture, Sports, Science and Technology of Japan (MEXT) through the MEXT projects Integrated Research Consortium on Chemical Sciences, Cooperative Research Program of Network Joint Research Center for Materials and Devices and Elements Strategy Initiative to Form Core Research Center, and by JST-CREST JPMJCR15P5 and JST-Mirai JPMJMI18A2. The computations in this work were primarily performed using computer facilities at the Research Institute for Information Technology, Kyushu University. Y.T. is grateful for a JSPS Grant-in-Aid for Scientific Research on Innovative Areas (Discrete Geometric Analysis for Materials Design, grant number JP20H04643, and Mixed Anion, grant number JP19H04700) and a Grant-in-Aid for Transformative Research Areas (A) “Supra-ceramics” (grant number JP22H05146).

References

1 A. J. Kinloch, The science of adhesion. *J. Mater. Sci.,* 1980, **15**, 2141–2166.
2 P. Edward, *Epoxy Adhesive Formulations*; McGraw-Hill Professional, 2005.
3 G. Fourche, *Polym. Eng. Sci.,* 1995, **35**, 968–975.
4 G. Fourche, *Polym. Eng. Sci.,* 1995, **35**, 957–967.
5 E. M. Petrie, Epoxy adhesives. *Epoxy Adhesive Formulations*; McGraw-Hill Education: New York, 2005; Chapter 1, pp 1–26.
6 J. Bai, Ed. *Advanced Fibre-Reinforced Polymer (FRP) Composites for Structural Applications*; Woodhead Publ. Oxford, 2013.
7 F. Ohsako and K. Yoshizawa, *Jpn. J. Polym. Sci. Tech*., 2011, **68**, 72–80.
8 T. Semoto, Y. Tsuji and K. Yoshizawa, *Bull. Chem. Soc. Jpn.,* 2012, **85**, 672–678.
9 T. Semoto, Y. Tsuji, H. Tanaka and K. Yoshizawa, *J. Phys. Chem. C,* 2013, **117**, 24830–24835.
10 K. Yoshizawa, T. Semoto, S. Hitaoka, C. Higuchi, Y. Shiota and H. Tanaka, *Bull. Chem. Soc. Jpn.,* 2017, **90**, 500–505.
11 D. J. Henry, G. Yiapanis, E. Evans and I. Yarovsky, *J. Phys. Chem. B,* 2005, **109**, 17224–17231.
12 S. Köppen, O. Bronkalla and W. Langel, *J. Phys. Chem. C,* 2008, **112**, 13600–13606.
13 S. Köppen and W. Langel, *Langmuir,* 2010, **26**, 15248–15256.
14 S. A. Mian, L. C. Saha, J. Jang, L. Wang, X. Gao and S. Nagase, *J. Phys. Chem. C,* 2010, **114**, 20793–20800.
15 S. A. Mian, L. M. Yang, L. C. Saha, E. Ahmed, M. Ajmal and E. Ganz, *Langmuir,* 2014, **30**, 6906–6914.
16 L. Agosta, G. Zollo, C. Arcangeli, F. Buonocore, F. Gala and M. Celino, *Phys. Chem. Chem. Phys*., 2015, **17**, 1556–1561.
17 G. Bahlakeh, M. Ghaffari, M. R. Saeb, B. Ramezanzadeh, F. De Proft and H. Terryn, *J. Phys. Chem. C,* 2016, **120**, 11014–11026.
18 S. Ogata and Y. Takahashi, *J. Phys. Chem. C,* 2016, **120**, 13630–13637.
19 K. Min, Y. Kim, S. Goyal, S. H. Lee, M. McKenzie, H. Park, E. S. Savoy, A. R. Rammohan, J. C. Mauro, H. Kim, K. Chae, H. S. Lee, J. Shin and E. Cho, *Polymer,* 2016, **98**, 1–10.
20 K. Min, A. R. Rammohan, H. S. Lee, J. Shin, S. H. Lee, S. Goyal, H. Park, J. C. Mauro, R. Stewart, V. Botu, H. Kim and E. Cho, *Sci. Rep*., 2017, **7**, 10475.
21 K. Yoshizawa, H. Murata and H. Tanaka, *Langmuir,* 2018, **34**, 14428–14438.
22 S. Ogata and M. Uranagase, *J. Phys. Chem. C,* 2018, **122**, 17748–17755.
23 C. Higuchi, H. Tanaka and K. Yoshizawa, *J. Comput. Chem*., 2019, **40**, 164–171.
24 Y. Tsuji, Y. Kitamura, M. Someya, T. Takano, M. Yaginuma, K. Nakanishi and K. Yoshizawa, *ACS Omega,* 2019, **4**, 4491–4504.
25 S. Nakamura, Y. Tsuji and K. Yoshizawa, *ACS Omega,* 2020, **5**, 26211–26219.
26 C. Higuchi and K. Yoshizawa, *Langmuir,* 2021, **37**, 8417–8425.
27 N. Tsurumi, Y. Tsuji, N. Masago and K. Yoshizawa, *ACS Omega,*

2021, **6**, 34173–34184.
28 Y. Tsuji, T. Baba, N. Tsurumi, H. Murata, N. Masago and K. Yoshizawa, *Langmuir,* 2021, **37**, 3982–3995.
29 R. K. Chitumalla, K. Kim, X. Gao and J. Jang, *Phys. Chem. Chem. Phys*., 2021, **23**, 1031–1037.
30 Y. Sumiya, Y. Tsuji and K. Yoshizawa, *ACS Omega,* 2022, **7**, 17393–17400.
31 S. Nakamura, S. Yamamoto, Y. Tsuji, K. Tanaka and K. Yoshizawa, *Langmuir,* 2022, **38**, 6653-6664.
32 K. Yamaguchi, D. Kawaguchi, N. Miyata, T. Miyazaki, H. Aoki, S. Yamamoto and K. Tanaka, *Phys. Chem. Chem. Phys*., 2022, **24**, 21578-21582.
33 A. Shundo, S. Yamamoto, K. Tanaka, *JACS Au,* 2022, **2**, 1522-1542.
34 H. Chang, L. Bu, G. Kong and R. Labayen, *The International Symposium on Power Semiconductor Devices and ICs*, 2011; pp 320–323.
35 M.-F. Shu and Y.-H. Tseng, *Int. Symp. Microelectron*., 2018, **2018**, 000161–000166
36 G. Kresse and J. Hafner, *Phys. Rev. B,* 1993, **47**, 558–561.
37 G. Kresse and J. Hafner, *Phys. Rev. B,* 1994, **49**, 14251–14269.
38 G. Kresse and J. Furthmüller, *Comput. Mater. Sci*., 1996, **6**, 15–50.
39 J. P. Perdew, K. Burke and M. Ernzerhof, *Phys. Rev. Lett.,* 1996, **77**, 3865–3868.
40 S. Grimme, J. Antony, S. Ehrlich and H. Krieg, *J. Chem. Phys*., 2010, **132**, 154104.
41 S. Grimme, S. Ehrlich and L. Goerigk, *J. Comput. Chem*., 2011, **32**, 1456–1465.
42 G. Kresse and D. Joubert, *Phys. Rev. B: Condens. Matter Mater. Phys.,* 1999, **59**, 1758–1775.
43 B. Adolph, J. Furthmüller and F. Beckstedt, *Phys. Rev. B: Condens. Matter Mater. Phys.,* 2001, **63**, No. 125108.
44 K. Momma and F. Izumi, *J. Appl. Crystallogr*., 2011, **44**, 1272–1276.
45 *Materials Studio 6.1*; Accelrys, Inc.: San Diego, CA, 2012.
46 H. Sun, *J. Phys. Chem. B,* 1998, **102**, 7338–7364.
47 B. Leimkuhler, E. Noorizadeh and F. A. Theil, *J. Stat. Phys.,* 2009, **135**, 261–277.
48 M. R. Pinnel, H. G. Tompkins and D. E. Heath, *Appl. Sur. Sci*., 1979, **2**, 558-577.
49 R. Al-Gaashani, S. Radiman, N. Tabet, A. R. Daud, *J. Alloys Comp*., 2011, **509**, 8761-8769.
50 M. M. Islam, B. Diawara, V. Maurice and P. Marcus, *J. Mol. Struct.,* 2009, **903**, 41–48.
51 A. Soon, M. Todorova, B. Delley and C. Stampfl, *Phys. Rev. B: Condens. Matter Mater. Phys.,* 2007, **75**, 125420.
52 X. Yu, X. Zhang, S. Wang and G. Feng, *Appl. Surf. Sci*., 2015, **343**, 33-40.
53 C. Moller and N. Nilius, *J. Phys. Chem. C,* 2017, **121**, 20877-20881.
54 H. Wu, N. Zhang, H. Wang and S. Hong, *Chem. Phys. Lett*., 2013, **568**, 84-89.
55 F. Muttaqien, Y. Hamamoto, I. Hamada, K. Inagaki, Y. Shiozawa, K. Mukai, T. Koitaya, S. Yoshimoto, J. Yoshinobu and Y. Morikawa, *J. Chem. Phys*., 2017, **147**, 094702.
56 M. Goland and E. Reissner, *J. Appl. Mech*., 1994, **11**, 17–27.
57 S. Akpinar, M. O. Doru, A. Ozel, M. D. Aydin and H. G. Jahanpasand, *Compos. Part B Eng. Els. Ltd*, 2013, **55**, 55-64.
58 F. L. Matthews, P. F. Kilty and E. W. Godwin, *Composites,* 1982, **13**, 29–37.
59 A. Calik, *Eng. Rev*. 2016, **36**, 29–34.
60 G. F. Ji, Z. Y. Ouyang, G. Q. Li, S. Ibekwe and S. S. Pang, *Int. J. Sol. Str*., 2010, **18**, 2445-2458.
61 A. W. Mello and K. M. Liechti, *J. Appl. Mech.-Trans. As*., 2006, **73**, 860-870.
62 K. Gall, M. F. Horstemeyer, M. Van Schilfgaarde and M. I. Baskes, *J. Mech. Phys. Sol*., 2000, **48**, 2183-2212.
63 S. Yang, F. Gao and J. Qu, *Polymer* 2013, **54**, 5064-5074.
64 R. Dronskowski and P. E. Bloechl, *J. Phys. Chem*., 1993, **97**, 8617-8624.
65 Y. Wu, C. He and W. Zhang, *J. Am. Chem. Soc*., 2022, **144**, 9344-9353.
66 F. Heslot, T. Baumberger, B. Perrin, B. Caroli and C. Caroli, *Phys. Rev. E,* 1994, **49**, 4973.
67 S. Fujisawa, Y. Sugawara, S. Ito, S. Mishima, T. Okada and S. Morita, *Nanotechnology,* 1993, **4**, 138.
68 M. Dienwiebel, N. Pradeep, G. S. Verhoeven, H. W. Zandbergen and J. W. M. Frenken, *Surf. Sci*., 2005, **576**, 197–211.
69 D. Mandelli, I. Leven, O. Hod and M. Urbakh, *Sci. Rep*., 2017, **7**, 10851.
70 P. K. Jana, W. Chen, M. J. Alava and L. Laurson, *Phys. Chem. Chem. Phys*., 2018, **20**, 18737–18743.
71 D. Mandelli, W. Ouyang, O. Hod and M. Urbakh, *Phys. Rev. Lett*., 2019, **122**, 076102.
72 A. Vanossi, C. Bechinger and M. Urbakh, *Nat. Comm*., 2020, **11**, 4657.
73 Z. He, Y. Zhu and H. Wu, *J. Mech. Phys. Sol*., 2022, **158**, 104560.